Influence of the Collision Energy on the $O(^1D) + RH \rightarrow OH(X^2\Pi) + R$ ($RH = CH_4$, C_2H_6, C_3H_8) Reaction Dynamics: A Laser-Induced Fluorescence and Quasiclassical Trajectory Study

Miguel González,*,† María P. Puyuelo,‡ Jordi Hernando,† R. Sayós,† Pedro A. Enríquez,‡ Javier Guallar,‡ and Irene Baños‡

Departament de Química Física i Centre de Recerca en Química Teòrica, Universitat de Barcelona, C/Martí i Franquès, 1. 08028 Barcelona, Spain, and Departamento de Química, Universidad de La Rioja, C/Obispo Bustamante, 3. 26004 Logroño, Spain

Received: February 26, 1999; In Final Form: August 16, 1999

The influence of the collision energy (E_T) on the $O(^1D) + RH \rightarrow OH(X^2\Pi) + R$ ($RH = CH_4$, C_2H_6, and C_3H_8) reaction dynamics has been studied, using the N_2O photodissociation at 193 nm as $O(^1D)$ precursor ($\langle E_T \rangle = 0.403$ eV) and probing the OH $v'' = 0$ and 1 levels by LIF. A triatomic QCT study of the reaction with CH_4 on a fully ab initio based analytical PES has also been performed, and a quite good agreement with the experimental OH rovibrational distributions has been obtained. Our experimental results are similar to those obtained when the O_3 photodissociation is used to produce $O(^1D)$ ($\langle E_T \rangle = 0.212$ eV), as expected on the basis of the available energy in products and also from the QCT calculations. The $P(v''=0)/P(v''=1)$ populations ratio values reported for C_2H_6 and C_3H_8 in a very recent work (Wada and Obi, *J. Phys. Chem. A* **1998**, *102*, 3481), where the N_2O was also used to generate $O(^1D)$, are probably largely underestimated. The rotational distributions obtained are similar to those obtained in other experiments, and a quite good agreement has been obtained for the spin−orbit and Λ-doublet populations. The reaction takes place near exclusively through the insertion of the $O(^1D)$ atom into a C−H bond below 0.6 eV, and the mechanism may be direct or nondirect (mainly through short-lived $(CH_3)OH$ collision complexes) with about the same probability. The OH vibrational distribution arising from the direct mechanism is inverted, while the nondirect one leads to a noninverted distribution. At higher E_T, the abstraction mechanism also contributes appreciably to reactivity.

I. Introduction

The reactions of the oxygen atom in the first excited electronic state, $O(^1D)$, with alkanes, and especially with CH_4, are relevant in stratospheric chemistry in the context of ozone degradation processes through the OH/HO_2 catalytic cycle.[1−3] Although most studies have focused on the reaction of $O(^1D)$ with CH_4, detailed information concerning the reactions with C_2H_6, C_3H_8, and $C(CH_3)_4$ is also available. The following exothermic reaction channel is considered here:

$$O(^1D) + RH \rightarrow OH(X^2\Pi) + R \qquad (1)$$

with $RH = CH_4$, C_2H_6, and C_3H_8 ($\Delta H^\circ_{r,298K}$ ranges from −43.1 ($R = CH_3$) to −52.6 ($R =$ iso-C_3H_7) kcal mol^{-1} [4]). In C_s symmetry, reactants correlate with products through two potential energy surfaces (PES), $^1A'$ and $^1A''$ PES, and the ground PES ($^1A'$) contains a deep minimum which corresponds to the ROH alcohol molecule (ROH enthalpy with respect to reactants ($\Delta H^\circ_{m,298K}$) ranges from −134.4 ($R = CH_3$) to −144.6 ($R =$ iso-C_3H_7) kcal mol^{-1} [4]).

Global (including all reaction channels) thermal rate constants for the reactions of $O(^1D)$ with alkanes generally fall near the gas kinetic values (CH_4,[5] C_2H_6,[6] and C_3H_8[6]). These reactions proceed with no activation energy, which suggests the absence of an energy barrier (including the zero-point energy (ZPE)) on the PES minimum energy path (MEP). This is in contrast with what happens for the analogous reactions with the ground state oxygen atom, $O(^3P)$. For the reaction of $O(^1D)$ with CH_4 at room temperature 90 (+10, −20)% of reactive processes lead to $OH(X^2\Pi) + CH_3(X^2A_2'')$.[7] The yield of the reaction channel leading to $OH(X^2\Pi)$ + alkyl radical is very much lower for larger alkanes. For C_2H_6, C_3H_8, and $C(CH_3)_4$, the observed yields for OH production relative to that for CH_4 are 0.033, 0.056, and 0.033, respectively.[8] For alkanes different from CH_4 the cleavage of the weaker C−C bond would predominate. From the measured H atom branching ratios and data of the literature, the yield of the reaction channels not producing OH, H, or the quenching of $O(^1D)$ atom has been estimated as 0.87 for C_2H_6 and 0.86 for C_3H_8.[6]

The measurement of the $OH(X^2\Pi)$ vibrational[8−14] and rotational[8−9,12−15] distributions arising from these reactions has been the object of several studies, using mainly laser-induced fluorescence (LIF) to probe this radical, allowing in some cases for rotational thermalization. The $O(^1D)$ was generated by photodissociation of N_2O (193 nm) or of O_3 (248 or 266 nm). The OH rovibrational energy substantially decreases when moving from CH_4 to larger alkanes. The $OH(X^2\Pi_{3/2})/OH(X^2\Pi_{1/2})$ spin−orbit population ratio is statistical,[8−9,12−14] and the $\Pi(A')/\Pi(A'')$ Λ-doublet population ratio is larger than 1 for CH_4, tending to decrease and becoming equal to 1 for larger alkanes.[8−9,12,14] The stereodynamics of the $O(^1D) + CH_4 \rightarrow OH$

* Corresponding author. E-mail: miguel@qf.ub.es.
† Universitat de Barcelona.
‡ Universidad de La Rioja.

10.1021/jp990691p CCC: $19.00
Published on Web 12/31/1999

+ CH_4 reaction has also been examined[16,17] using polarized Doppler-resolved LIF spectroscopy.

For the $O(^1D) + CH_4$ system, the formation of CH_3,[18−19] the reaction channels producing H,[6,20−21] H_2,[21] CH_2O, $^1CH_2$, and $O(^3P)$,[7] and the reaction from the $CH_4 \cdot O_3$ van der Waals (vdW) complex photodissociated at 267 nm[22] have been considered. In addition, the reactions of $O(^1D)$ with clusters of simple alkanes have also been studied.[12]

From a theoretical point of view, there is an ab initio study at the CASSCF and CCI levels on the $^1CH_2 + H_2O$, $H_2 + HCOH$, and $H_2 + H_2CO$ channels, which may follow the fragmentation of CH_3OH,[23] and an ab initio study at the CASSCF and MRCI levels on the $O(^1D) + CH_4$ reaction emphasizing the $OH + CH_3$ and $CH_3O + H$ channels.[24]

This work follows a previous contribution carried out in our laboratory,[13] where the N_2O photodissociation at 193 nm was used to generate $O(^1D)$ for the first time in the context of these reactions and study the influence of collision energy on the dynamics. The $O(^1D) + RH \rightarrow OH(X^2\Pi) + R$ ($RH = CH_4$, C_2H_6, and C_3H_8) reactions have been investigated, probing the $v'' = 0$ and 1 OH vibrational levels by LIF, and determining the rotational, spin−orbit, and Λ-doublet populations. A quasiclassical trajectory (QCT) study of the $O(^1D) + CH_4$ reaction dynamics, in the framework of a fully ab initio triatomic model, has also been performed. This allows for a strong interaction between experiment and theory. At this point, it is worth to remark that, once the experiments reported here were finished, an experimental work appeared[14] where the same reactions and a similar experimental methodology were considered. Since there are important differences between our results and those of ref 14, mainly in what respects the OH vibrational distribution for $v'' = 0$ and 1 resulting from C_2H_6 and C_3H_8, we have performed additional and careful checks of our results and experimental procedure. The experiments and data analysis were carried out adequately and, in particular, there were no polarization or saturation problems. To open the possibility of a wider verification, taking into account results reported in other laboratories on related systems, we have also studied the OH($v'' = 0$, 1) molecules produced from the $O(^1D) + C_2H_4$ reaction. A good agreement with all experimental data (rovibrational, spin−orbit, and Λ-doublet populations) reported for the reaction with C_2H_4 in a previous work[25] has been found. Besides the present QCT results suggest that the amount of OH($v'' = 0$) produced with respect to that of OH($v'' = 1$) given in ref 14 for C_2H_6 and C_3H_8 is largely underestimated. A more detailed discussion on these topics will be given in section III.

II. Methodology

II.1. Experimental Method. Experiments were carried out in a laser photolysis−LIF setup employing a flow system (Figure 1). High purity gases furnished by Praxair were used without further purification (N_2O (99.998%), CH_4 (99.995%), C_2H_6 (99.99%), and C_3H_8 (99.95%)). The N_2O and alkane gases were flowed into a stainless steel chamber pumped by a rotary pump (Leybold HV350, 30 m^3/h). A partial pressure of 45 mTorr was used for both gases. The total pressure was controlled by three needle valves and monitored by a capacitance manometer (Leybold CM1). The $O(^1D)$ atom was generated by photodissociation of N_2O at 193 nm using an ArF excimer laser (Lambda-Physik Compex 100). The quantum states of OH($X^2\Pi$, v'', N'', F'', λ'') were detected by LIF exciting the (0, 0) and (1, 1) diagonal bands of the $A^2\Sigma^+ \leftarrow X^2\Pi$ transition (306−318 nm wavelength region) with a XeCl-pumped tunable dye laser (Lambda-Physik LPX 105i and LPD 3002 CES (sulforhodamine B), respectively). The output frequency was doubled with a KDP crystal and the resulting wavelengths were passed through an Oriel UG5 filter. The photolysis and dye laser beams counterpropagated collinearly and both lasers were operated at 11 Hz. The low total pressure and short time delay between the two lasers ($\Delta t = 250$ ns), allowed to determine the quantum states of OH with a minimal relaxation by collisions. On average, only about 1−2 collisions were suffered by the OH molecules before being detected. Estimations indicate that the possible corrections due to the rotational relaxation of $OH(A^2\Sigma^+)$ by collisions with N_2O and alkanes fall within the experimental error margin and, as in previous works,[8,13−14] no correction was made. The intensity of the unresolved $A^2\Sigma^+ \rightarrow X^2\Pi$ fluorescent emission was collected by a lens placed at 90° with respect to the laser beams and focused on a photomultiplier tube (Hamamatsu R1398) through two Oriel UG11 and two Corion SB-300-F filters. The output signals were amplified five times (Stanford SR-240 preamplifier), integrated (Stanford SR-250 integrator), and after A/D conversion (Stanford SR-245 converter) transfered into a personal computer. These signals were corrected adequately from intensity variations in the photolysis and dye lasers, which were monitored with photodiodes (Hamamatsu S1336-18BQ and S1336-5BQ, respectively) and integrated simultaneously using two integrators (Stanford SR-250). Another photodiode (Hamamatsu S1722-029) was used to trigger the LIF signal boxcar integrator. The LIF signal intensity depended linearly from the power of both the photolysis and dye lasers. Line assignments for the OH(A−X) transition were performed using the data of ref 26. An example of LIF excitation spectra is shown in Figure 2 (R_{11} branch of the (0,0) and (1,1) bands of the $OH(X^2\Pi)$ molecule). The OH populations in the four rovibrational fine structure states were derived from the LIF signal intensity using tabulated Einstein *B* coefficients.[27] The main lines of the P, Q, and R branches were employed to determine populations. For branches where main lines and satellites overlap, their sum was determined and separated into components from the ratio of Einstein *B* coefficients. Lines that partially overlap were deconvoluted by fitting with separate Gaussian functions according to a nonlinear least-squares procedure. The populations of high rotational levels of $v'' = 0$

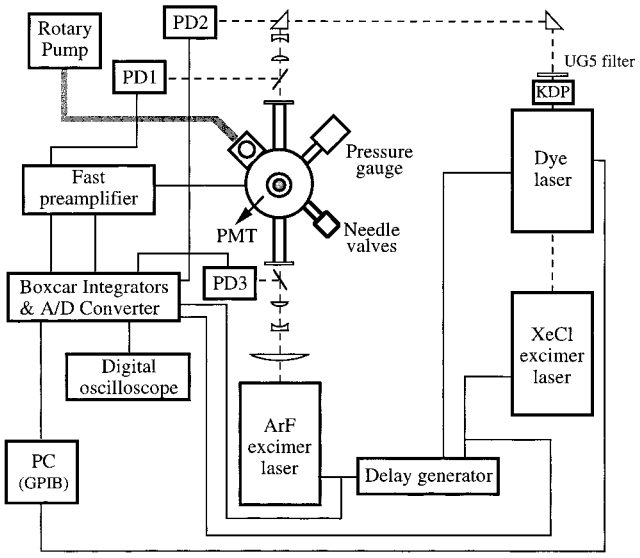

Figure 1. Schematic representation of the experimental setup. Two photodiodes (PD1 and PD2) were used, respectively, to measure the power of the dye laser beam and to trigger the LIF signal boxcar integrator. The power of the ArF excimer laser was measured employing the PD3 photodiode or using the photomultiplier (PMT).

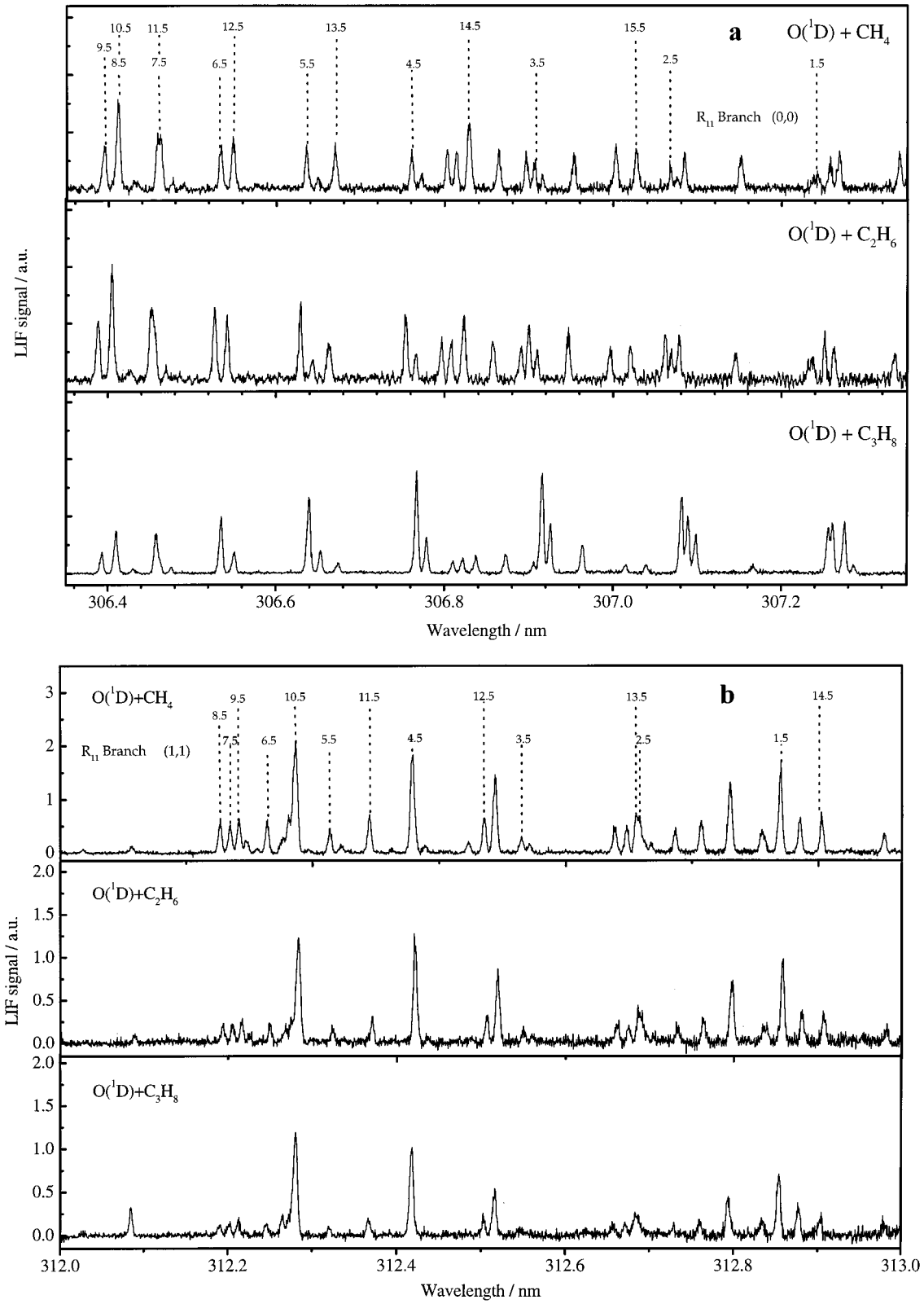

Figure 2. LIF excitation spectra (R_{11} branch): (a) (0,0) and (b) (1,1) band regions of the nascent OH for the three reactions considered.

and $v'' = 1$, which cannot be determined by LIF since they are affected by predissociation of the $A^2\Sigma^+$ state,[28] were estimated as in ref 8 by extrapolating the linear rotational surprisals to the thermochemical limits.

II.2. Theoretical Method. The dynamics of the simplest reaction considered, i.e., that with CH_4, has been studied theoretically using the QCT method[29] as implemented in the TRIQCT program,[30] employing a triatomic analytical function (available from the authors upon request),[31] fully based on ab initio calculations, to represent the ground PES. This model, which treats the CH_3 group as a pseudoatom of 15 amu placed in its center of mass ($O(^1D) + H-(CH_3) \rightarrow OH + (CH_3)$, $O-(CH_3) + H$), has also been used successfully in our laboratory recently for the analogous reaction with $O(^3P)$.[32]

As a detailed description of the ab initio calculations and analytical function fitted has been reported elsewhere,[31] only a

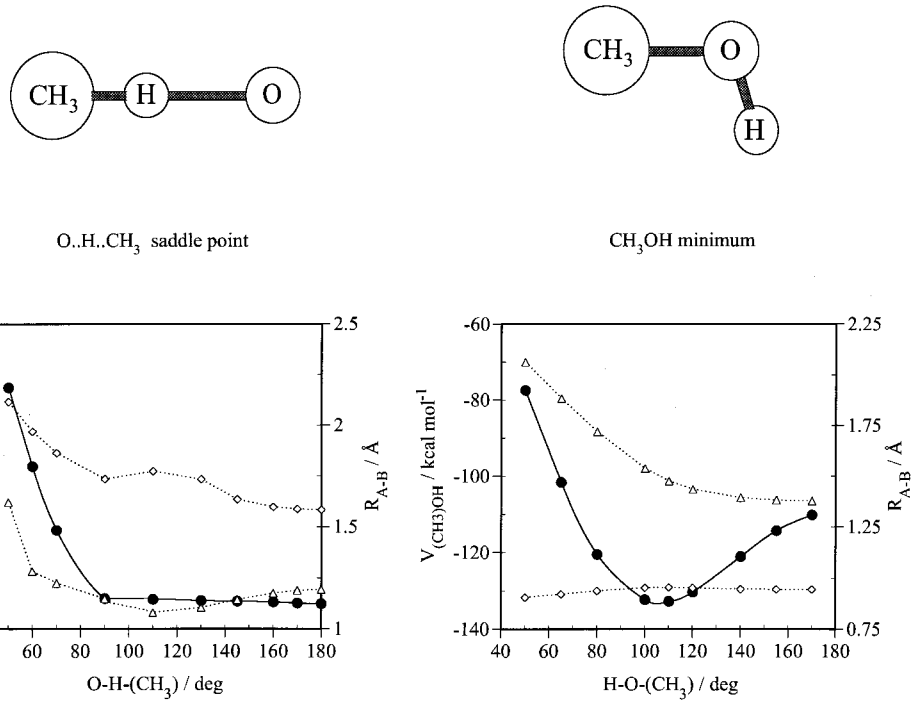

Figure 3. Saddle point and minimum structures on the analytical triatomic PES, and dependence of the energy (●) and geometry of both stationary points as a function of the O−H−(CH_3) and H−O−(CH_3) angles, respectively. Distances (R_{A-B}) are the following: O−H (◇) and H−(CH_3) (△) for the saddle point; O−H (◇) and O−(CH_3) (△) for the minimum.

brief summary about them will be given here. The ground PES of the O(^{1}D) + CH_4 system (^{1}A′ PES in C_s) has been characterized at the PUMP4//UMP2 Møller−Plesset ab initio level with the 6-311G(2df, 2pd) basis set. The geometry and energy of reactants, the two possible products asymptotes of the triatomic model, the CH_3OH alcohol minimum, the $OHCH_3$ saddle point, and additional points connecting all the stationary points and in other regions of the PES have been calculated. The 126 ab initio points calculated (geometries and energies) were fitted, within the framework of the above-mentioned triatomic model, using the same type of analytical representation (many-body expansion) considered in previous reactions studied by our group (e.g., N(^{4}S) + NO,[33] O(^{3}P) + CS,[34] H(^{2}S) + Cl_2 and Cl(^{2}P) + HCl,[35] N(^{4}S) + O_2,[36] and O(^{3}P) + H−(CH_3)[32] reactions). The saddle-point and minimum structures together with the corresponding angular dependence of the energy and geometry on the triatomic analytical PES are plotted in Figure 3.

Two main collision energies (E_T, relative translational energy) have been considered (0.403 and 0.212 eV) in the QCT calculations. The former corresponds to the average O(^{1}D) + CH_4 E_T value arising when the O(^{1}D) is produced from N_2O photodissociation at 193 nm, while the latter is that one from the O_3 photodissociation at 248 nm. QCT calculations have also been performed at $E_T = 0.6$ and 0.8 eV to obtain a deeper insight into the influence of the translational energy on the reaction dynamics. The rovibrational distribution of the H−(CH_3) pseudodiatomic molecule was sampled in both cases from a Maxwell−Boltzmann distribution at $T = 298$ K. An initial distance of 10 Å between the O(^{1}D) atom and the center of mass of the H(CH_3) molecule and an integration step of 0.25×10^{-16} s were considered.

To compare the QCT rotational populations with the experimental data, as the QCT method includes neither the orbital ($\Lambda = 1$) nor the spin ($S = {}^1/_2$) electronic angular momenta of the OH($X^2\Pi$) molecule, we have identified N'', the total angular momentum quantum number (excluded the electronic and nuclear spins), to $j'' + 1$, where j'' is the rotational angular momentum quantum number. In what follows, however, when considering the rotational levels of OH, as usual, we will refer to N''.

III. Results and Discussion

III.1. Rovibrational Populations. The OH($X^2\Pi$) $v'' = 0$ and 1 rovibrational populations have been measured by means of the LIF technique for the three reactions considered here: O(^{1}D) + CH_4, C_2H_6, and C_3H_8 (Table 1). The same properties for $v'' = 0-4$ and O(^{1}D) + CH_4 have been calculated using the QCT method at two collision energies (0.403 and 0.212 eV) (Table 2). Hence, it is possible to compare theoretical results with experimental data obtained when the photodissociations of N_2O at 193 nm (this work and refs 13 and 14) and O_3 at 248 nm (refs 8 and 10) are used, respectively, as O(^{1}D) precursors. In Table 2 the results obtained at $E_T = 0.6$ and 0.8 eV are also shown.

The generation of O(^{1}D) atoms using two different precursors allows the influence of collision energy on dynamics, and in particular on the internal states distribution of the nascent OH molecule, to be studied. Even though there is only about 9% of difference between the corresponding available energies in products when the O(^{1}D) is generated by photodissociation of N_2O (193 nm) or O_3 (248 or 266 nm), the QCT calculations show the existence of significant differences in the rovibrational distributions. The QCT $[P(v'')]_{0.403\ eV}/[P(v'')]_{0.212\ eV}$ ratio for $v'' = 0-4$ is equal to 1.18, 1.02, 0.90, 0.90, and 1.00, respectively. Hence, when E_T evolves from 0.212 to 0.403 eV, an increase of 18% in $P(v'')$ occurs for $v'' = 0$, while a decrease of about 10% in $P(v'')$ takes place for both $v'' = 2$ and 3. $P(v'' = 1)$ exhibits nearly the same values at both collision energies, as it also happens for $v'' = 4$.

For O(^{1}D) + CH_4, a good agreement is found between the experimental results, if error margins are included. The $P(v''=0)/P(v''=1)$ ratio is around 1.0. The consideration of the experi-

TABLE 1: Experimental Vibrational Populations and Average Rotational Levels of the OH ($X^2\Pi$) Molecule Arising from the $O(^1D) + RH \rightarrow OH + R$ Reaction (RH = Alkane)

		$P(v'')/P(v''=1)$ and $\langle N'' \rangle_{v''}$ [a]				
RH	study	$v''=0$	$v''=1$	$v''=2$	$v''=3$	$v''=4$
CH_4	N_2O−193 nm					
	this work	1.44 ± 0.38	1.00			
		(12.7 ± 1.2)	(12.7 ± 1.5)			
	ref 14	0.92	1.00			
	O_3−248 nm					
	ref 8	1.00	1.00	1.32	0.47	0.19
		(13.6)	(12.8)	(12.4)	(8.8)	(6.4)
	ref 10[b]		1.00	1.22	0.97	0.52
C_2H_6	N_2O−193 nm					
	this work	2.03 ± 0.39	1.00			
		(10.5 ± 0.9)	(13.1 ± 1.1)			
	ref 14	1.27	1.00			
	O_3−248 nm					
	ref 8	2.50	1.00	0.70	0.43	0.38
		(9.9)	(12.6)	(10.0)	(7.9)	(5.3)
C_3H_8	N_2O−193 nm					
	this work	4.94 ± 0.64	1.00			
		(6.0 ± 1.0)	(12.6 ± 0.9)			
	ref 14	2.33	1.00			
	O_3−248 nm					
	ref 8	4.70	1.00	1.25	0.83	0.92
		(6.4)	(11.3)	(11.1)	(10.2)	(5.4)

[a] The first value appearing for each study and vibrational level corresponds to the $P(v'')/P(v''=1)$ ratio, and the one in parentheses gives the average rotational level. [b] OH rotationally relaxed.

mental data together with the QCT results allows for a better understanding of the dynamics. If the QCT $P(v'')/P(v''=1)$ ratios for $v'' = 0-4$ at $E_T = 0.212$ eV are compared with the experimental data from O_3 photodissociation at 248 nm,[8,10] a quite good agreement is found (the agreement with ref 8 being almost excellent); a relatively flat peaked at $v'' = 2$ distribution is observed for the nascent $OH(X^2\Pi)$ radical. The QCT distribution for $E_T = 0.403$ eV is somewhat different from the above-mentioned one. The distribution is again relatively flat between $v'' = 0-3$ but peaking at $v'' = 0$ in this case. This tendency to obtain higher populations for $v'' = 0$ than for $v'' = 1$ as collision energy increases found in the calculations is also observed in the experimental results reported here, although in the former case the increase is lower than in experiments. The increase of $v'' = 0$ population reported here contrasts with the tendency measured in ref 14, although both results agree if error margins are taken into account. The QCT value of the $P(v''=0)/P(v''=1)$ ratio is approximately equidistant between the present experimental result and that of ref 14. The QCT vibrational populations for $v'' = 0-3$ at $E_T = 0.6$ and 0.8 eV are very close to the ones for 0.403 eV, being substantially larger for $v'' = 4-6$. Hence, above ca. 0.4 eV, the OH vibrational energy content increases with E_T. The average vibrational energy levels are 1.8, 1.7, 1.9, and 2.1 for $E_T = 0.212$, 0.403, 0.6, and 0.8 eV, respectively.

As a general tendency, an increase in the value of the $P(v''=0)/P(v''=1)$ ratio is observed as the size of the hydrocarbons increase. The experimental $OH(X^2\Pi)$ $P(v''=0)/P(v''=1)$ ratios reported here for C_2H_6 and C_3H_8 show a strong disagreement with those reported in ref 14. The values measured here are about twice the ones reported in ref 14, but similar to the ratios measured when the O_3 photodissociation, at 248 nm[8] and 266 nm,[9] is used as $O(^1D)$ precursor. From the present experimental and theoretical results and taking into account previous experimental data,[8−9] it seems reasonable to conclude that the $P(v''=0)/P(v''=1)$ populations ratio values for C_2H_6 and C_3H_8 reported in ref 14 are largely underestimated.

The QCT OH rotational distributions arising from $O(^1D) + CH_4$ have quite similar shapes for $E_T = 0.212$ and 0.403 eV, but for 0.403 eV they tend to populate higher N'' values. The QCT rotational distributions at 0.403 and 0.212 eV reproduce the shapes of the present experimental data and that of ref 8. Nevertheless, while experimental measurements do not suggest an appreciable effect of E_T on the rotational distributions, QCT calculations show that OH rotational energy increases with E_T. As E_T increases from 0.212 to 0.403 eV, on average an increase of 26% occurs in $\langle N'' \rangle v''$ from the QCT calculations, this being in the interval 15% ($v''=0$) to 41% ($v'' = 4$). Also, from both theory and experiments, it comes out that rotational energy decreases as vibrational energy increases. This occurs in a significant extent although, as indicated before, there is a small change (about 9%) in the available energy in products. The above-indicated tendencies in what regards the QCT rotational distributions are also observed at 0.6 and 0.8 eV.

The experimental rotational distributions for $OH(X^2\Pi, v''=0)$ and $OH(X^2\Pi, v''=1)$ produced by the reaction $O(^1D) + CH_4$ measured here (Figure 4) are quite close to those of ref 8. In ref 14, it was indicated that the rotational distributions they measured were similar to those of ref 8. The analysis of the rotational surprisals reveals that the present rotational energy distributions are bimodal, this being particularly clear for $v'' = 0$ as in ref 8. This bimodal character was also reported in ref 14 for both $v'' = 0$ and $v'' = 1$. It is possible to distinguish low and high N'' components in the rotational distribution. The high N'' and low N'' components of the $OH(v''=0)$ level resulting from CH_4, C_2H_6, and C_3H_8 can be well reproduced considering rotational temperatures (T_{rot}) of 10 700 and 1300 K, 11 000 and 1050 K, and 8500 and 650 K, respectively. In general, these results are in reasonable agreement with those of ref 14 (12 600 and 960 K, 12 500 and 1100 K, and 12 900 and 820 K, respectively) but differ from that of ref 8 (9800 and 500 K, 5900 and 1200 K, and 4700 and 600 K, respectively). QCT results for $OH(v''=0)$ from $O(^1D) + CH_4$ at $E_T = 0.212$ eV also show bimodality but not at 0.403 eV. T_{rot} in these cases are 11 483 and 2509 K and 13 500 K, respectively. The influence of the microscopic reaction mechanism on the energy distribution in products will be considered in section III.4.

III.2. Spin−Orbit Populations. The spin−orbit interaction in $OH(X^2\Pi)$ leads to the existence of two electronic fine structure states, F_1 and F_2 ($X^2\Pi_{3/2}$ and $X^2\Pi_{1/2}$, respectively). The lowest lying F_1 electronic state has been probed by the $P_{11}(N'')$, $Q_{11}(N'')$, and $R_{11}(N'')$ transitions, and the F_2 by the $P_{22}(N'')$, $Q_{22}(N'')$, and $R_{22}(N'')$. The spin−orbit population ratio, $P(v'', N'', X^2\Pi_{1/2})/P(v'', N'', X^2\Pi_{3/2})$, as a function of N'', and the average $P(v'', N'', X^2\Pi_{3/2})N''/P(v'', N'', X^2\Pi_{1/2})(N'' + 1)$ ratios for $v'' = 0$ and 1 obtained here are shown in Figure 5 and Table 3, respectively. The $P(v'', N'', X^2\Pi_{1/2})/P(v'', N'', X^2\Pi_{3/2})$ ratio is generally not far from the corresponding statistical value, $N''/(N'' + 1)$, but there is some tendency to populate preferentially the lowest lying $X^2\Pi_{3/2}$ state. This is probably in agreement with previous experimental data,[8−9,13−14] although no preferential population of either electronic fine structure state was reported, if error margins are taken into account. On the contrary, for the OH molecules produced in the analogous reactions of $O(^3P)$ with alkanes, a preferential population of the $X^2\Pi_{3/2}$ state has been reported.[37−38] The reactions of $O(^3P)$ involve different PES than in the $O(^1D)$ case, and in contrast to what happens for the latter reactions (cf. section III.4), the former ones take place via H atom abstraction through a direct reaction mode.[32,37−38]

TABLE 2: Theoretical Vibrational Populations and Average Rotational Levels of the OH ($X^2\Pi$) Molecule Arising from the $O(^1D) + CH_4 \rightarrow OH + CH_3$ Reaction[a]

	$P(v'')/P(v''=1)$ and $\langle N'' \rangle_{v''}$						
E_T/eV	$v''=0$	$v''=1$	$v''=2$	$v''=3$	$v''=4$	$v''=5$	$v''=6$
0.212[b]	0.97 ± 0.03	1.00 ± 0.03	1.09 ± 0.03	0.98 ± 0.03	0.48 ± 0.02		
	(14.4 ± 1.3)	(13.2 ± 1.1)	(12.5 ± 0.9)	(10.1 ± 0.7)	(6.8 ± 0.6)		
0.403[c]	1.12 ± 0.03	1.00 ± 0.03	0.96 ± 0.03	0.87 ± 0.03	0.47 ± 0.02	0.07 ± 0.01	
	(16.9 ± 1.6)	(16.5 ± 1.6)	(15.0 ± 1.4)	(13.4 ± 1.2)	(9.8 ± 1.1)	(5.5 ± 1.7)	
0.6	1.14 ± 0.06	1.00 ± 0.05	0.93 ± 0.05	0.81 ± 0.04	0.67 ± 0.04	0.18 ± 0.01	
	(19.4 ± 2.1)	(18.5 ± 2.0)	(16.9 ± 1.8)	(15.0 ± 1.6)	(12.1 ± 1.4)	(7.5 ± 1.6)	
0.8	1.13 ± 0.06	1.00 ± 0.05	0.89 ± 0.05	0.87 ± 0.05	0.83 ± 0.04	0.33 ± 0.02	0.04 ± 0.01
	(21.2 ± 2.3)	(20.4 ± 2.3)	(19.0 ± 2.1)	(17.0 ± 1.8)	(14.0 ± 1.5)	(9.8 ± 1.6)	(5.2 ± 1.9)

[a] The first value appearing for each study and vibrational level corresponds to the $P(v'')/P(v''=1)$ ratio, and the one in parentheses gives the average rotational level. [b] Average E_T when the $O(^1D)$ atoms are generated by photodissociation of O_3 at 248 nm. [c] Average E_T when the $O(^1D)$ atoms are generated by photodissociation of N_2O at 193 nm.

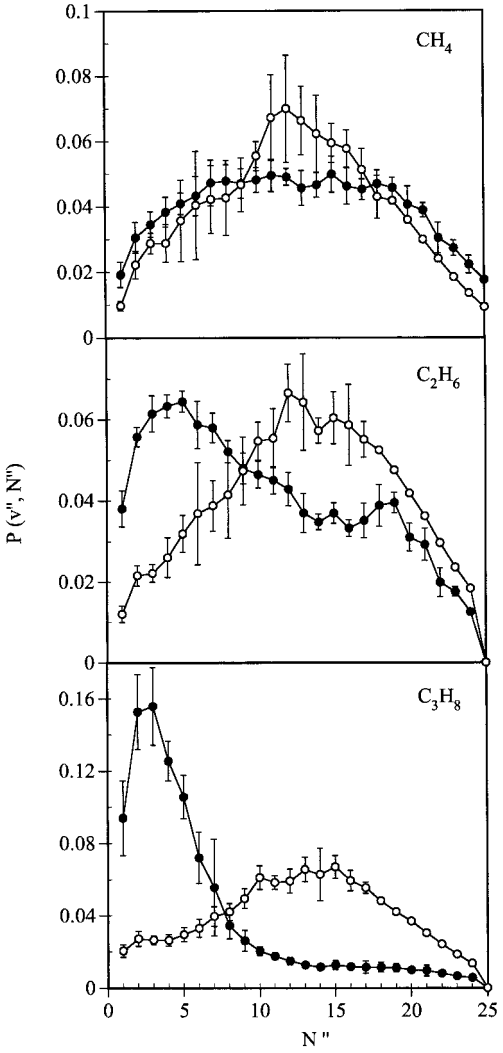

Figure 4. LIF rotational populations for $OH(v''=0)$ (●) and $OH(v''=1)$ (○) from the reactions of $O(^1D)$ with CH_4, C_2H_6, and C_3H_8. Populations are normalized so that for $v''=0$ the sum extended over all populated rotational levels is equal to 1. This is also the case for $v''=1$ when the corresponding sums for CH_4, C_2H_6, and C_3H_8 are multiplied, respectively, by 1.4, 2.0, and 4.9. Error bars correspond to one standard deviation.

III.3. Λ-Doublet Populations. Two Λ-doublet fine structure states, $\Pi(A')$ and $\Pi(A'')$, arise from the interaction of electronic orbital and rotational angular momenta. In the high rotational levels limit case the $\Pi(A')$ state corresponds to the alignment of the half-filled π OH molecular orbital in the rotation plane, while a perpendicular alignment of this orbital to that plane occurs for the $\Pi(A'')$ state. The $\Pi(A')$ state population has been determined from the P and R transitions and the $\Pi(A'')$ population from the Q transitions. The Λ-doublet populations ratio as a function of N'' (Figure 6) and the average ratios for

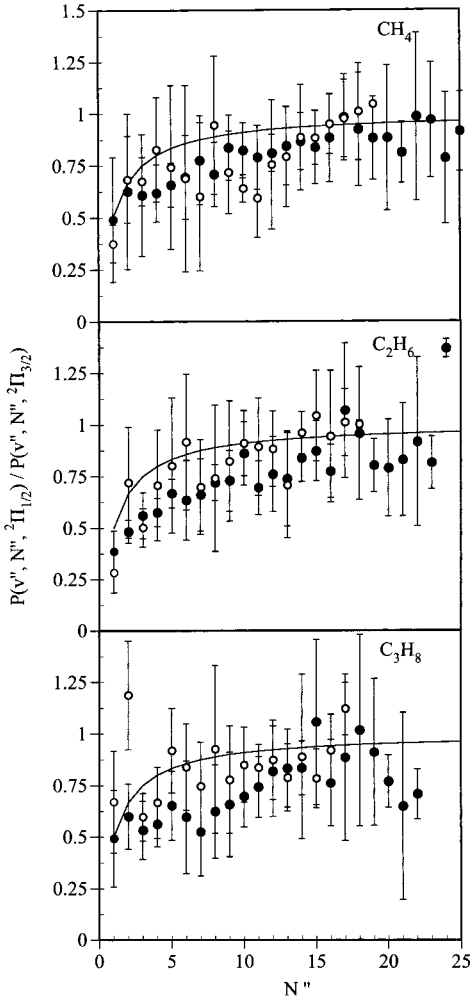

Figure 5. LIF spin−orbit populations ratio for $OH(v''=0)$ (●) and $OH(v''=1)$ (○) from the reactions of $O(^1D)$ with CH_4, C_2H_6, and C_3H_8. Error bars correspond to one standard deviation.

TABLE 3: Experimental Average Spin−Orbit State Populations Ratio of the OH ($X^2\Pi$) Molecule Arising from the $O(^1D) + RH \rightarrow OH + R$ Reaction (RH = Alkane)

	$P(F_1)N''/P(F_2)(N''+1)$	
RH	$v''=0$	$v''=1$
CH_4	1.11 ± 0.21	1.16 ± 0.29
C_2H_6	1.18 ± 0.25	1.11 ± 0.28
C_3H_8	1.24 ± 0.47	1.03 ± 0.24

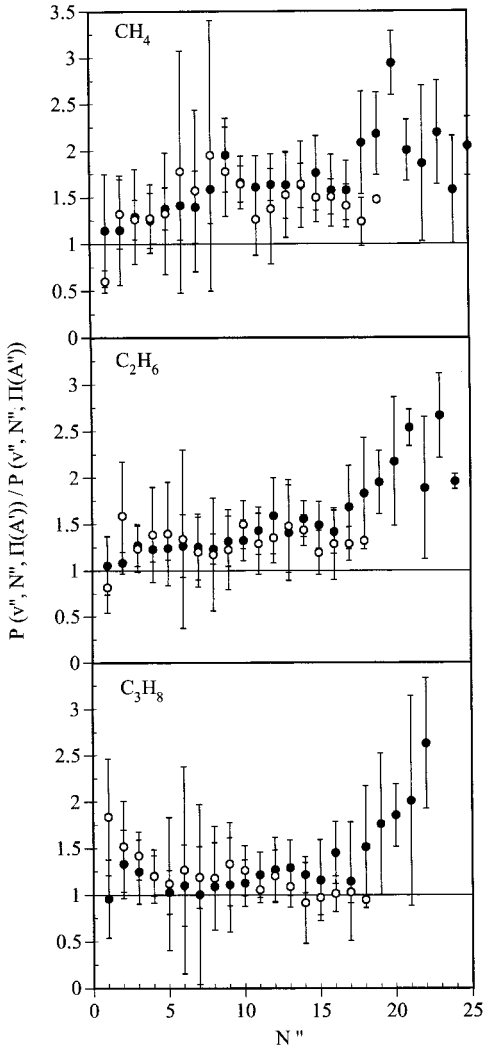

Figure 6. LIF lambda doublet populations ratio for OH(v''=0) (●) and OH(v''=1) (○) from the reactions of O(^{1}D) with CH_4, C_2H_6, and C_3H_8. Error bars correspond to one standard deviation.

TABLE 4: Experimental Average Λ-Doublet Fine Structure State Populations Ratio of the OH ($X^2\Pi$) Molecule Arising from the O(^{1}D) + RH → OH + R Reaction (RH = Alkane)

	$P(\Pi(A'))/P(\Pi(A''))$	
RH	$v''=0$	$v''=1$
CH_4	1.66 ± 0.35	1.47 ± 0.35
C_2H_6	1.43 ± 0.29	1.33 ± 0.29
C_3H_8	1.20 ± 0.24	1.10 ± 0.20

$v''=0$ and 1 (Table 4) show a preferential population of the $\Pi(A')$ state. This trend diminishes from CH_4 to C_3H_8 and from $v''=1$ to $v''=0$. In general, very similar results have also been obtained by other authors.[8−9,14] Nevertheless, quite higher values have been reported in ref 14 for C_2H_6 and C_3H_8 in $v''=0$, and particularly high is the value given in ref 12 for CH_4 in $v''=1$. The preferential population of $\Pi(A')$ over $\Pi(A'')$ is usually explained on the basis of a reaction mechanism where the OH rotation follows a preferential orientation during the fragmentation of the R−O−H bent collision complex. The decrease of $\Pi(A')$ preferential population as the size of the alkane increases can be attributed on a reasonable basis to the existence of a progressively less well defined plane of fragmentation in the collision complex. The decrease of $\Pi(A')$ preferential population as the vibrational level increases from $v''=0$ to $v''=1$ seems to correlate with the more nondirect character (more short-lived collision complexes formation with geometries around that of the CH_3OH minimum) of the reactive trajectories leading to $v''=0$ (cf. section III.4). For the OH molecules produced in the analogous reactions of O(^{3}P) with alkanes, however, no preferential population of either Λ-doublet states was reported.[37−38] This is not surprising as for these reactions the OH distributions are dominated by the lowest rotational levels.

III.4. Microscopic Reaction Mechanism. The microscopic reaction mechanism of the reaction O(^{1}D) + H−(CH_3) → OH + (CH_3) at E_T = 0.212, 0.403, 0.6, and 0.8 eV has been studied analyzing the reactive trajectories obtained in the QCT calculation (about 18 000 reactive trajectories for 0.212 and 0.403 eV and about 7000 for the higher energies). The (CH_3)OH deep alcohol minimum plays an essential role in the dynamics, as most reactive trajectories take place through geometries close to this minimum (insertion mechanism). The abstraction mechanism (direct reaction mode), that is clearly minor, only accounts for more than 1% of the reactivity at 0.6 eV (3.5%) and 0.8 eV (8.3%). The reactive trajectories evolving close to the (CH_3)-OH minimum, can be classified in two groups. The first group refers to situations where the (CH_3)OH collision complex lifetime can be considered as negligible (direct reaction insertion mechanism). The second group involves collision complexes (mainly short-lived) that exist during several vibrational periods (nondirect reaction insertion mechanism). These two groups of reactive trajectories have essentially the same contribution to the insertion mechanism. The lifetimes of the collision complexes are within the intervals 0.03−1.83 ps (average value of 0.20 ps) and 0.04−2.33 ps (average value of 0.18 ps) for, respectively, 0.212 and 0.403 eV. Around 80% of nondirect reactive insertion trajectories evolve through (CH_3)OH collision complexes that exist during less than 0.30 ps. Because of these short lifetime values, energy randomization is not allowed. Similar results are also found for 0.6 and 0.8 eV, the average lifetime values being 0.18 and 0.17 ps, respectively.

The QCT average lifetime obtained here probably corresponds to a lower limit of the theoretical value which would be obtained after consideration of all degrees of freedom, and cannot be compared with the experimental half-collision result of ref 22 (3 ps), due to the very different initial conditions (geometry, energy, and angular momentum) explored. From a chemical quenching experiment where the O(^{1}D) atoms were generated by N_2O photolysis at 185 nm, an average lifetime of 0.8 ps was estimated.[39] However, this experiment has some important uncertainties, e.g., it was not determined whether the O(^{1}D) atoms were thermalized before reacting with CH_4. Because of these uncertainties and the different nature of the experiments reported in refs 22 and 39, the large discrepancy between both lifetimes is not surprising.

The dependence of the OH vibrational distribution with E_T and the microscopic mechanism is shown in Figure 7. The vibrational distribution from the direct reaction insertion mechanism is inverted and has a maximum at $v''=2$ for 0.212−0.6 eV, while it is noninverted for 0.8 eV. However, the corresponding one for the nondirect reactive trajectories is noninverted in all cases. In what concerns the abstraction reaction mode, which has some importance at 0.6 and 0.8 eV, the vibrational distribution is strongly inverted and peaks at $v''=4$. Regarding the OH rotational distributions, the most relevant results mainly refer to the $v''=0-1$ levels. There is a tendency to give broader rotational distributions peaking at higher N'' values in the case of the nondirect trajectories. For $v''=0$ this behavior is responsable of the bimodal rotational distribution obtained in the QCT calculations at 0.212 eV. For all populated

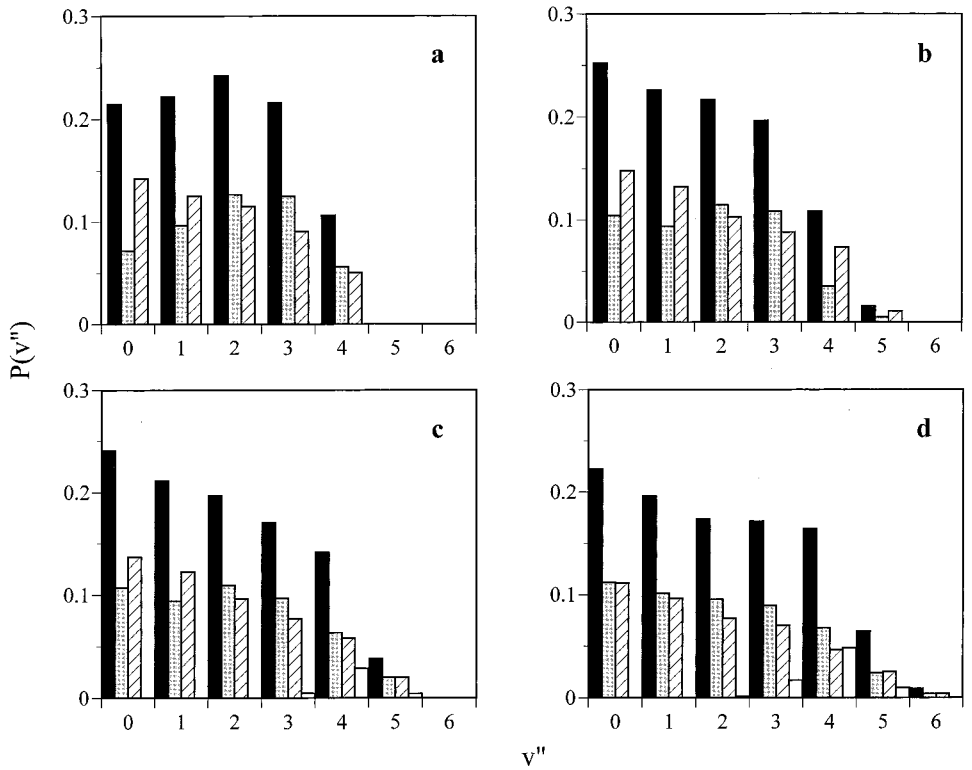

Figure 7. QCT OH vibrational populations arising from the reaction of $O(^1D)$ with CH_4 at four collision energies: (a) $E_T = 0.212$ eV; (b) $E_T = 0.403$ eV; (c) $E_T = 0.6$ eV; (d) $E_T = 0.8$ eV. Black, gray, crosshatched, and white histograms are the vibrational distributions corresponding to, respectively, all reactive trajectories, direct reactive insertion trajectories, nondirect reactive insertion trajectories, and reactive abstraction trajectories. For each vibrational level, the sum of populations associated with the different microscopic mechanisms gives the global one.

v'', the average rotational level, $\langle N'' \rangle$, is in general somewhat larger for nondirect reactive trajectories than for the direct ones. This is particularly evident for $v'' = 0$ and 1 (0.212 eV) and $v'' = 0$ (0.403, 0.6, and 0.8 eV). The analysis of the OH rovibrational distribution as a function of the collision complex lifetime does not reveal the existence of significant differences.

IV. Conclusions

The influence of the collision energy (E_T) on the $O(^1D) + RH \rightarrow OH(X^2\Pi) + R$ ($RH = CH_4$, C_2H_6, and C_3H_8) reaction dynamics has been investigated, using the N_2O photodissociation at 193 nm as $O(^1D)$ precursor and probing the $OH(X^2\Pi)$ $v'' = 0$ and 1 levels by laser-induced fluorescence (LIF), and determining the OH rovibrational, spin−orbit, and Λ-doublet populations. A triatomic quasiclassical trajectory (QCT) dynamics study of the reaction with CH_4 (CH_3 group treated as a pseudoatom of 15 amu) on a fully ab initio based analytical representation (many-body expansion) of the ground potential energy surface (PES),[31] available from the authors upon request, has also been performed. The QCT study has been mainly focused on the determination of the $OH(X^2\Pi, v''=0-4, N'')$ rovibrational distributions for $E_T = 0.403$ and 0.212 eV. The former corresponds to the average $O(^1D) + CH_4$ E_T value arising when the $O(^1D)$ is produced from N_2O photodissociation at 193 nm, while the latter is that one from the O_3 photodissociation at 248 nm. A quite good agreement between the QCT and experimental data has been obtained. Besides, additional calculations have been carried out at $E_T = 0.6$ and 0.8 eV to obtain a deeper insight into the reaction dynamics.

The $P(v''=0)/P(v''=1)$ vibrational populations ratio for CH_4 obtained in different laboratories (present work and refs 8, 9, and 14) are essentially in agreement once error margins are included. However, the values reported here for C_2H_6 and C_3H_8 show a strong disagreement with those reported in a recent work carried out in similar conditions,[14] where also the N_2O photodissociation was used to generate $O(^1D)$, but are quite similar to the ratios measured when the O_3 photodissociation is used as a $O(^1D)$ precursor.[8−9] The agreement between our results and those obtained from the O_3 photodissociation is expected on the basis of the available energy in products and also from the QCT calculations. Hence, it seems reasonable to conclude that the $P(v''=0)/P(v''=1)$ values for C_2H_6 and C_3H_8 reported in ref 14 are largely underestimated. The rotational distributions obtained in different experiments are similar, and a quite good agreement has been obtained for the spin−orbit and Λ-doublet populations. In contrast to the reactions of $O(^1D)$ with alkanes studied here, the analogous reactions with $O(^3P)$ show a preferential population of the $X^2\Pi_{3/2}$ state and no preferential population of either Λ-doublet states.

The analysis of the reactive trajectories obtained in the QCT calculations has allowed the microscopic reaction mechanism of the $O(^1D) + CH_4$ reaction to be characterized. For 0.212 and 0.403 eV, the reaction takes place nearly exclusively through the insertion of the $O(^1D)$ atom into a C−H bond and the resulting trajectories may be direct or nondirect (mainly through short-lived $(CH_3)OH$ collision complexes) with about the same probability. At the higher energies considered, however, the abstraction mechanism also has some contribution to reactivity (3.5% at 0.6 eV and 8.3% at 0.8 eV). In general, the OH vibrational distributions arising from the direct insertion mechanism are inverted, while the nondirect one leads to noninverted distributions. The vibrational distributions resulting from the abstraction mechanism are strongly inverted and peak at high v'' levels. There is some tendency to give broader OH rotational

distributions peaking at higher N'' values, particularly for the vibrational levels $v'' = 0-1$, in the case of the nondirect trajectories.

Acknowledgment. This work has been supported by the "Dirección General de Enseñanza Superior (DGES)" of the Spanish Ministry of Education and Culture (MEC) through the Projects DGES PB95-0598-C02-01 and PB95-0598-C02-02. J.H. thanks the CIRIT from the "Generalitat de Catalunya" (Autonomous Government) for a Ph. D. Studentship. The authors are also grateful to the University of La Rioja and "Generalitat de Catalunya" (ref 1998SGR 00008) for partial support, to Mr. Luis Zorzano and Mr. Rodrigo Martínez for their help, and to Profs. Pedro J. Campos, Antonio Aguilar, and Fernando Castaño for their permanent encouragement.

References and Notes

(1) Wiesenfeld, J. R. *Acc. Chem. Res.* **1982**, *15*, 110.
(2) Warneck, P. *Chemistry of the natural atmosphere*; Academic Press: San Diego, 1988.
(3) Burnett, E. B.; Burnett, C. R. *J. Atmos. Chem.* **1995**, *21*, 13.
(4) Chase, M. W., Jr.; Davies, C. A.; Downey, J. R., Jr.; Frurip, D. J.; McDonald, R. A.; Syverud, A. N. *J. Phys. Chem. Ref. Data* **1985**, *14* (Suppl. 1).
(5) Atkinson, R.; Baulch, D. L.; Cox, R. A.; Hampson, R. F., Jr.; Kerr, J. A.; Troe, J. *J. Phys. Chem. Ref. Data* **1992**, *21*, 1215.
(6) Matsumi, Y.; Tonokura, K.; Inagaki, Y.; Kawasaki, M. *J. Phys. Chem.* **1993**, *97*, 6816.
(7) Hack, W.; Thiesemann, H. *J. Phys. Chem.* **1995**, *99*, 17364.
(8) Park, C. R.; Wiesenfeld, J. R. *J. Chem. Phys.* **1991**, *95*, 8166.
(9) Luntz, A. C.; *J. Chem. Phys*. **1980**, *73*, 1143.
(10) Aker, P. M.; O'Brien, J. J. A.; Sloan, J. J. *J. Chem. Phys.* **1986**, *84*, 745.
(11) Cheskis, S. G.; Iogansen, A. A.; Kulakov, P. V.; Razuvaev, I. Yu.; Sarkisov, O. M.; Titov, A. A. *Chem. Phys. Lett.* **1989**, *155*, 37.
(12) Rudich, Y.; Hurwitz, Y.; Frost, G. J.; Vaida, V.; Naaman, R. *J. Chem. Phys.* **1993**, *99*, 4500.
(13) González, M.; Hernando, J.; Sayós, R.; Puyuelo, M. P.; Enríquez, P. A.; Guallar, J.; Baños, I. *Faraday Discuss.* **1997**, *108*, 453.
(14) Wada, S.; Obi, K. *J. Phys. Chem.* **1998**, *102*, 3481.
(15) Brouard, M.; Duxon, S. P.; Simons, J. P. *Isr. J. Chem.* **1994**, *34*, 67.
(16) Brouard, M.; Simons, J. P. The stereodynamics of photon initiated bimolecular reactions. In *The chemical dynamics and kinetics of small radicals, Part II*; Liu, K., Wagner, A., Eds.; World Scientific: Singapore, 1995; p 795.
(17) Simons, J. P. *J. Chem. Soc., Faraday Trans.* **1997**, *93*, 4095.
(18) Suzuki, T.; Hirota, E. *J. Chem. Phys.* **1993**, *98*, 2387.
(19) Schott, R.; Schlütter, J.; Olzmann, M.; Kleinermanns, K. *J. Chem. Phys.* **1995**, *102*, 8371.
(20) Brownsword, R. A.; Hillenkamp, M.; Schmiechen, P.; Volpp, H.-R.; Upadhyaya, H. P. *J. Phys. Chem.* **1998**, *102*, 4438.
(21) Lin, J. J.; Harich, S.; Lee, Y. T.; Yang, X. *J. Chem. Phys*. **1999**, *110*, 10821.
(22) van Zee, R. D.; Stephenson, J. C. *J. Chem. Phys.* **1995**, *102*, 6946.
(23) Walch, S. P.; *J. Chem. Phys.* **1993**, *98*, 3163.
(24) Arai, H.; Kato, S.; Koda, S. *J. Phys. Chem.* **1994**, *98*, 12.
(25) Honma, K.; *J. Chem. Phys*. **1993**, *99*, 7677.
(26) Stark, G.; Brault, J. W.; Abrams, M. C. *J. Opt. Soc. Am. B* **1994**, *11*, 3.
(27) Chidsey, I. L.; Crosley, D. R. *J. Quantum. Spectrosc. Radiat. Transfer* **1980**, *23*, 187.
(28) Brzozowski, J.; Erman, P.; Lyyra, M. *Phys. Scr.* **1978**, *17*, 507.
(29) Raff, L. M.; Thompson, D. L. In *Theory of chemical reaction dynamics*; Baer, M., Ed.; CRC Press: Boca Raton, 1985; Vol. 3, p 1.
(30) Sayós, R.; González, M. *TRIQCT* (unpublished program).
(31) González, M.; Hernando, J.; Baños, I.; Sayós, R. *J. Chem. Phys.* **1999**, *111*, 8913.
(32) González, M.; Hernando, J.; Millán, J.; Sayós, R. *J. Chem. Phys.* **1999**, *110*, 7326.
(33) Gilibert, M.; Aguilar, A.; González, M.; Mota, F.; Sayós, R. *J. Chem. Phys.* **1992**, *97*, 5542.
(34) González, M.; Hijazo, J.; Novoa, J. J.; Sayós, R. *J. Chem. Phys.* **1996**, *105*, 10999.
(35) González, M.; Hijazo, J.; Novoa, J. J.; Sayós, R. *J. Chem. Phys.* **1998**, *108*, 3168.
(36) Sayós, R.; Hijazo, J.; Gilibert, M.; González, M. *Chem. Phys. Lett.* **1998**, *284*, 101.
(37) Andresen, P.; Luntz, A. C. *J. Chem. Phys.* **1980**, *72*, 5842.
(38) Sweeney, G. M.; Watson, A.; McKendrick, K. G. *J. Chem. Phys.* **1997**, *106*, 9172.
(39) Lin, C.-L.; DeMore, W. B. *J. Phys. Chem.* **1973**, *77*, 863.